Microscopic theory of the low frequency Raman modes in germanium nanocrystals

Wei Cheng,[1,2] Shang-Fen Ren,[2] and Peter Y. Yu[3]
[1]*Key Laboratory in University for Radiation Beam Technology and Materials Modification, Institute of Nuclear Physics, Beijing Normal University, Beijing, 100875, People's Republic of China*
[2]*Department of Physics, Illinois State University, Normal, Illinois 61790-4560, U.S.A.*
[3]*Department of Physics, University of California, Berkeley, and Materials Sciences Division, Lawrence Berkeley National Laboratory, Berkeley, California 94720, U.S.A.*
(Received 13 October 2004; published 25 May 2005)

We have studied the Raman intensities of low-frequency phonon modes in germanium (Ge) nanocrystals (NC) with varying sizes by using a microscopic valence force field model. The results are compared with the predictions of the continuum model of Lamb using a projection method. We found that the $l=0$ spheroidal Lamb modes are Raman active in the parallel polarization scattering geometry, while the $l=2$ spheroidal Lamb modes are active in the crossed polarization geometry. This result agrees with the group theory prediction that the torsional Lamb modes are *not* Raman active, but is in disagreement with the identification of torsional Lamb modes in the crossed polarization Raman spectra of NC suggested by many authors.

DOI: 10.1103/PhysRevB.71.174305 PACS number(s): 63.22.+m, 81.05.Cy, 78.30.−j

I. INTRODUCTION

Quantum dots and nanocrystals (NC) have attracted great interest in recent years both for their fundamental science[1] and potential applications. In particular, as the size of NC decreases, the ratio of atoms located at or near the surface of the NC increases dramatically. Surface atoms are subject to forces different from those in the interior of NC, so their vibrational properties are different, and their interaction with electrons confined in the NC is also expected to be different.

So far there are practically no experimental techniques which can measure directly the surface phonons in NC using either electrical or optical measurements. In principle, a low-temperature inelastic electron scanning tunneling microscope can be a sensitive technique for investigating surface phonon modes in NC and their interaction with electrons. Until these experiments can be performed, low-frequency ($10-20$ cm^{-1}) Raman scattering experiments are the only experimental results available for comparisons between theory. Such low-frequency Raman modes in spherical NC of various semiconductors embedded in glasses have been reported, for example, in NC of Ge (Ref. 2) and CdS (Ref. 3) embedded in GeO_2 glass, and in CdSSe doped silica-based glasses.[4] One characteristic of these Raman modes is that their frequency scales linearly with the inverse of the diameter of the NC. They have typically been interpreted as the spheroidal and torsional vibration modes of a continuum elastic sphere whose properties have been calculated by Lamb.[5] According to this model, the frequencies of these spheroidal and torsional modes are quantized in terms of two quantum numbers: a branch number n and the angular momentum l. Since the model assumes the NC to be an elastic continuum, it is expected to be valid only for large NC, but not for nm-sized NC containing, say, less than 1000 atoms.

In this paper, we have calculated the Raman spectra of low-frequency phonon modes of Ge NC containing 885 to 7289 atoms (largest diameter $d\sim 6.8$ nm) by applying a Raman polarizability model to the phonon modes computed with a microscopic valence force field model (VFFM).[6] Our results on the phonon density of states in Ge NC have already appeared in a brief report.[7] In the present paper, we also compare the computed Raman intensities of the phonon modes with the Raman selection rules of the Lamb modes. We found that for the large NC (i.e., $d\sim 6.8$ nm) the microscopic results agree well with the Raman selection rules of the continuum model based on group theory. However, for small NC (such as when $d<4$ nm) the continuum model breaks down. Our results indicate that the identification of torsional modes in the Raman spectra of NC proposed by many authors is erroneous.

This paper is organized in the following way. In the next section, we describe our theoretical approach; in Sec. III we show our calculated results and compare with existing experimental data; and in Sec. IV we summarize and conclude.

II. THEORETICAL APPROACHES

A. Valence force field model (VFFM)

The theoretical model used to investigate phonon modes in Ge NC is the VFFM,[6] developed to calculate phonon modes in semiconductor NC and quantum dots (QDs) in recent years.[8–13] In this model, the change of the total energy due to the lattice vibration is described by the following:[6]

$$E=\frac{1}{2}\sum_i C_0\left(\frac{\Delta d_i}{d_i}\right)^2+\frac{1}{2}\sum_j C_1(\Delta\theta_j)^2, \tag{1}$$

where C_0 and C_1 are two parameters that describe, respectively, the change in the total energy due to changes in the bond length and the bond angle, and the summation is over all the bond lengths and bond angles. To simplify the diagonalization of the dynamic matrix, the vibration modes of the NC are classified according to the point-group symmetry of the structure (tetrahedral or T_d for Ge). This allows us to study the NC vibrational modes belonging to different irreducible representations. One of the limitations of this model

is that it cannot reproduce both the sound velocity and the zone-boundary acoustic phonon frequency accurately at the same time. Since we focus on the phonons in the low-frequency range in this study, we used the Ge parameters (C_0=47.7 and C_1=2.8 eV) (Ref. 6) obtained by fitting the elastic constants.

B. Displacement vectors of spheroidal and torsional Lamb modes

In order to compare the NC modes calculated by VFFM with the Lamb modes, we need the analytical forms of the displacements of the Lamb modes. For ease of reference the derivations are summarized below.

Lamb's theory begins with the equation of motion for the displacement vector $\vec{D}$ of a three-dimensional elastic continuum spherical body with density ρ

$$\rho\partial^2\vec{D}/\partial^2 t = (\lambda + \mu)\,\nabla\,(\nabla\cdot\vec{D}) + \mu\nabla^2\vec{D}. \tag{2}$$

The two Lamb constants λ and μ are related to the longitudinal (v_l) and transverse (v_t) sound velocities of the continuum by $v_l=\sqrt{(\lambda+2\mu)/\rho}$, $v_t=\sqrt{\mu/\rho}$.

The spheroidal modes are defined by displacement vectors $\vec{D}_{lu}^{(S)}$

$$\vec{D}_{lu}^{(S)} = \nabla\,\phi_S + \alpha\,\nabla\times\nabla\times\vec{A}, \tag{3}$$

where α is a constant determined by the stress-free boundary condition, ϕ_s and $\vec{A}$ are, respectively, scalar and vector functions, defined by

$$\phi_S = j_l(hr)P_l^m(\cos\theta)\begin{Bmatrix}\cos m\phi\\ \sin m\phi\end{Bmatrix}\exp\{-i\omega t\},$$

in spherical coordinates (r,θ,ϕ) and

$$\vec{A} = (x\phi_V, y\phi_V, z\phi_V),$$

in Cartesian coordinates with

$$\phi_V = j_l(kr)P_l^m(\cos\theta)\begin{Bmatrix}\cos m\phi\\ \sin m\phi\end{Bmatrix}\exp\{-i\omega t\}.$$

In the above definitions ω is the vibration frequency, j_l(r) are the spherical Bessel functions, P_l^m are the Legendre polynomials indexed by the angular momentum numbers l and m. The subscript u in Eq. (3) is related to m by $u=m+l+1$ and runs from 1 to $2l+1$. The torsional modes are defined by displacement vectors $\vec{D}_{lu}^{(T)}$

$$\vec{D}_{lu}^{(T)} = \nabla\times\vec{A}. \tag{4}$$

In the above definitions the parameters h and k have the dimensions of wave vectors and are related to the longitudinal and transverse sound velocity by $h=\omega/v_l$ and $k=\omega/v_t$. Under a stress-free boundary condition the mode frequencies ω are determined by the solution of the following equations. For torsional modes, $\eta=kR$ (where R is the radius of the sphere) has to satisfy

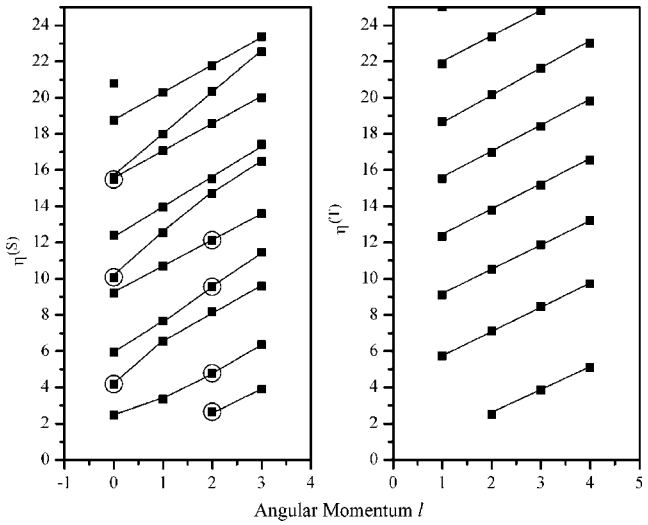

FIG. 1. Calculated values of η for both spheroidal (S) and torsional (T) Lamb modes as a function of the angular momentum number l. The solid lines join modes with the same branch number n (a special case: join l=1, n branch to l=2, n+1 branch). η increases with n in the sequence of $n=0,1,2\ldots$. Note that the values of η for the spheroidal mode are specific for Ge, with the choice of transverse and longitudinal sound velocities given in the text. The modes indicated with circles are found to be Raman active by projection onto our N=7289 atom Ge NC as discussed in the text.

$$d[j_{l+1}(\eta)/j_l(\eta)]/d\eta = 0. \tag{5}$$

The η values for torsional modes do not depend on materials and are universal. On the other hand, the frequencies of spheroidal modes depend on both h and k, which have to satisfy the following relation (with $\xi=hR$):

$$\begin{aligned}2[\eta^2 + (l-1)(l+2)\{\eta j_{l+1}(\eta)/j_l(\eta) - (l+1)\}]\xi j_{l+1}(\xi)/j_l(\xi)\\ - 0.5\eta^4 + (l-1)(2l+1)\eta^2 + \{\eta^2 - 2l(l-1)(l+2)\}\\ \times\eta j_{l+1}(\eta)/j_l(\eta) = 0.\end{aligned} \tag{6}$$

In this case the solutions η depend on the material through the ratio (v_l/v_t). For the torsional modes under a stress-free boundary condition the values of η are discrete and therefore the values of ω are usually labeled in increasing values by a integer n (branch number)=0,1,2... and the angular momentum number l.

By solving Eqs. (5) and (6) for the averaged values of the longitudinal and transverse speeds $v_l=5.25\times10^5$ cm/s and $v_t=3.25\times10^5$ cm/s appropriate for Ge, we have obtained η of Ge NC numerically for different values of n and l. The lowest values of η for both spheroidal and torsional modes are shown as a function of l in Fig. 1. The curves are arranged with increasing values of n starting with n=0. Because we have assumed a stress-free boundary condition, the η values for both spheroidal and transverse Lamb modes are quantized as shown in Fig. 1. In real samples the NC are often embedded in a matrix and, as a result, their surfaces are not stress-free. Thus, η may vary with external stress and may not be the same as those shown in Fig. 1. As a result, the frequency of the corresponding Lamb modes will also be

different. More discussions on η and the corresponding Lamb modes frequencies will be presented elsewhere. The modes enclosed by circles in Fig. 1 are Raman active. Before discussing the Raman intensity of these modes, we will first consider the displacement vectors of some lower-order Lamb modes.

(1) *Displacements of spheroidal* $l=0$ *mode*:

Neglecting the constant and time-dependent terms, we can write the scalar functions of the $l=0$ spheroidal modes as $\phi_S=j_0(hr)$, $\phi_V=j_0(kr)$. From Eq. (3) we obtain the displacement vectors

$$\vec{D}_{01}^{(S)} = -h\frac{j_1(hr)}{r}(x\vec{e}_x + y\vec{e}_y + z\vec{e}_z). \tag{7}$$

A simple group theory analysis shows that this mode belongs to the A_1 irreducible representations of the T_d group.

Displacements of $l=1,2$ spheroidal modes are summarized in Appendixes A and B.

(2) *Displacements of torsional* $l=1$ *modes*:

There are three orthogonal torsional modes that form a complete set of bases. Neglecting constants and time-dependent terms, their displacement vectors can be derived from $\phi_V=xj_1(kr)/r$ by substituting it into the expression for $\vec{A}$ and then using Eq. (4) to obtain

$$\vec{D}_{11}^{(T)} = -z\frac{j_1(kr)}{r}\vec{e}_y + y\frac{j_1(kr)}{r}\vec{e}_z. \tag{8}$$

Similarly, from $\phi_V=yj_1(kr)/r$ and $\phi_V=zj_1(kr)/r$ we obtain, respectively

$$\vec{D}_{12}^{(T)} = -x\frac{j_1(kr)}{r}\vec{e}_z + z\frac{j_1(kr)}{r}\vec{e}_x, \tag{9}$$

and

$$\vec{D}_{13}^{(T)} = -y\frac{j_1(kr)}{r}\vec{e}_x + x\frac{j_1(kr)}{r}\vec{e}_y. \tag{10}$$

These $l=1$ Lamb modes can be shown to form a set of complete orthogonal bases by satisfying the following equations:

$$\int\int\int \vec{D}_{11}^{(T)}\cdot\vec{D}_{11}^{(T)}dV = \int\int\int \vec{D}_{12}^{(T)}\cdot\vec{D}_{12}^{(T)}dV = \int\int\int \vec{D}_{13}^{(T)}\cdot\vec{D}_{13}^{(T)}dV,$$

$$\int\int\int \vec{D}_{11}^{(T)}\cdot\vec{D}_{12}^{(T)}dV = \int\int\int \vec{D}_{12}^{(T)}\cdot\vec{D}_{13}^{(T)}dV = \int\int\int \vec{D}_{11}^{(T)}\cdot\vec{D}_{13}^{(T)}dV = 0.$$

They belong to the triply degenerate T_1 representation of the T_d group.

Displacements of torsional $l=2$, and 3 modes are summarized in Appendixes C and D.

C. Projection of lattice modes onto Lamb modes

We can compare the displacement vectors obtained from the Lamb model and from the VFFM for discrete lattices by projecting the atomic displacements of the NC modes along the Lamb mode displacements. Since the displacements of Lamb modes are continuous functions of space within a sphere of radius R while the vibration amplitudes of lattice modes are discrete, all integrals over Lamb modes have to be replaced by summation over discrete lattice points. In addition, the vibration amplitudes are normalized to 1 in the same way as the vibrational amplitudes of NC obtained by the VFFM are presented. We then sum the *projection* of all the atoms in the NC and then square the sum to arrive at a quantity that we label as the *mode projection quantity*, or MPQ. For example, suppose the displacement vector of a NC lattice mode at an atom a is $\vec{V}(a)$, while the displacement at the same site of a spheroidal $l=0$ Lamb mode is $\vec{D}_{01}^{(S)}(a)$; then, the projection of the lattice mode onto the spheroidal Lamb mode is given by $s(a)=\vec{V}(a)\cdot\vec{D}_{01}^{(S)}(a)$. After we sum $s(a)$ over all the atoms in the NC and then square, we obtain $\mathrm{MPQ}=[\Sigma_a s(a)]^2$. This definition can be easily extended to Lamb modes with $l>0$, where the Lamb mode is defined by $2l+1$ vectors.

MPQ is a measure of the "similarity" between a NC lattice mode and a Lamb mode when the NC is treated as a spherical continuum. It is equal to 1 exactly if all NC atoms have exactly the same displacements as the Lamb mode at the same positions. On the other hand, if we project a NC mode onto a Lamb mode whose symmetry is not compatible with it the MPQ is then zero. Thus, for a given NC lattice mode, if we can find a Lamb mode with a MPQ value that is both maximum and close to 1, we can conclude that this lattice mode is almost identical to a Lamb mode. In such cases we will label the lattice mode as a "NC Lamb mode" and its frequency as a NC Lamb frequency.

D. Raman selection rule and intensities

As discussed in Ref. 14, the spheroidal Lamb modes transform according to the following irreducible representations of the rotational group $O(3)$: $D_g^{(0)}$, $D_u^{(2)}$, $D_g^{(2)}$, …, while the torsional Lamb modes transform as: $D_g^{(1)}$, $D_u^{(1)}$, $D_g^{(3)}$, …. From the group theory and the matrix element theorem,[15] one can show that only spheroidal Lamb modes with $l=0,2$ are Raman active.[14,15] This selection rule is in agreement with the results of Brillouin scattering experiments in large NC where indeed only these modes are observed.[16] However, torsional Lamb modes have been claimed to be observed experimentally with strength comparable to spheroidal modes.[2] One way to explain this result is that the so-called torsional modes in the experimental spectra are actually $l=2$ spheroidal modes with frequencies close to the torsional modes. Another possible explanation is that the Raman selection rule is not valid for small NC. For example, if we treat the Ge NC as composed of discrete atoms with local symmetry belonging to the T_d group, then from group theory we would derive the Raman selection rule for the T_d group: namely, that the A_1, E, and T_2 modes are all Raman

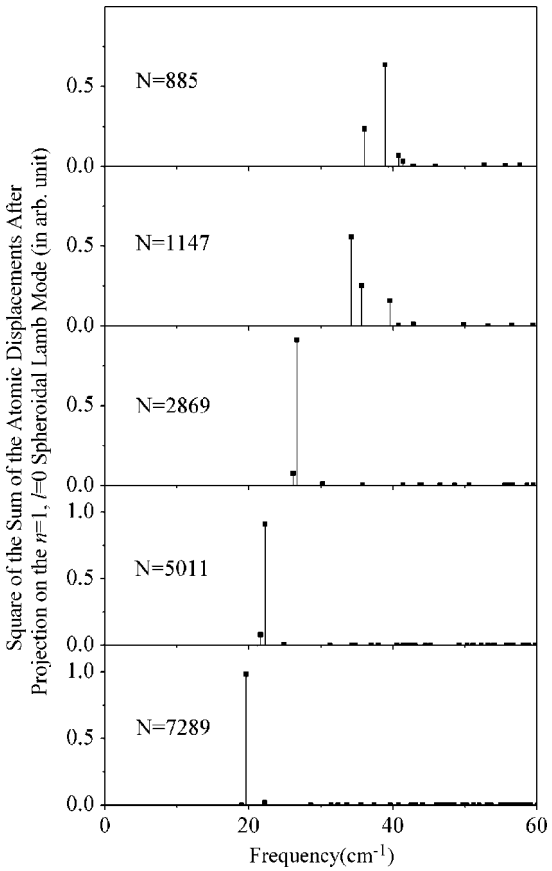

FIG. 2. Mode projection quantity (MPQ) for $n=1$ and $l=0$ spheroidal Lamb modes. Note that as N becomes less than 2869 (corresponding to $d\sim 4.9$ nm), the Lamb modes start to become composed of more than one lattice mode, although the mode frequencies continue to follow the $1/d$ dependence as long as $d>4$ nm, as discussed in the text.

active. By treating the NC as composed of discrete lattices, one will obtain a different set of Raman selection rules. Using the projection method, one can determine the Raman selection of Lamb modes based on the compatibility relation between the $O(3)$ and T_d groups. Using this approach, one can show that the spheroidal modes with $l=0$, 1, 2, and so on all contain Raman-active lattice modes, while only the $l=2,3,\ldots$ torsional modes contain Raman-active lattice modes. These selection rules, however, do not predict the strengths of the Raman modes except when they are zero. For example, the Raman-active torsional modes may be much weaker than those of the spheroidal modes. To compute the Raman intensities of the lattice modes, we have employed the bond-polarizability approximation discussed in a previous paper.[12] Using this model we have obtained the Raman intensities of lattice modes in Ge NC containing 885 to 7289 atoms.

III. RESULTS AND DISCUSSION

A. Projection of lattice modes onto Lamb modes

In Figs. 2–4 we show the computed values of MPQ (defined in Sec. II C) for five Ge NCs with different number of atoms in the NC. In Fig. 2, all the NC modes are projected onto the spheroidal Raman-active ($n=1$, $l=0$) Lamb mode. From this figure, we see that when the number of atoms is greater than 2869, the NC modes with the maximum component of Lamb modes contain a single major peak whose strength is greater than 80%. This suggests that, for large NC, the lower-order spheroidal Lamb modes are also eigenmodes of the discrete lattice. However, when the number of atom is less than 1147, the Lamb mode contains two or more lattice modes, although there is still a dominant contribution from one mode whose strength can be as large as 65%. The transition from only one dominant lattice mode in the projection to several modes seems to occur rather suddenly. In the case of Ge NC we found that this occurs at a "critical" diameter (d) of about 4.0 nm.[7] Below this size it is no longer possible to derive the frequency of the Lamb modes from the VFFM since several modes of different frequencies contribute to the Lamb mode. One way to understand this result is to note that the frequency of the spheroidal $l=0$ Lamb mode depends on both longitudinal and transverse sound speeds. In the microscopic lattice model, the longitudinal and transverse sound speeds vary with the direction of propagation. Thus, when the Lamb mode is composed of modes propagating along different directions these modes will have slightly different frequencies. In such cases, the frequency of the mode with the maximum MPQ will still satisfy approximately the linear dependence on ($1/d$) as discussed in Ref. 7.

In Fig. 3, we select a small and a large NC and separately plot the projection of their lattice modes onto the torsional Lamb modes [with $n=0$ and $l=2$ (a), $l=3$ (b), and $l=4$ (c), respectively. The results for the $l=1$ mode are not shown since it is Raman inactive] according to their irreducible representations. One should note the drastic change in the vertical scale from a mode with one symmetry to another in these plots. From these figures we conclude that, in general, only a mode with a specific symmetry among the five possible ones dominates the Lamb mode both for large and small NC. For example, for the $l=2$ torsional mode it is the E symmetry modes, while for the $l=3$ torsional mode it is modes with T_2 symmetry. The Lamb components in other symmetries are too small to be significant. This suggests that the compatibility relation between the $O(3)$ and T_d groups can be a guide to predict the relative magnitude of the projection of the lattice modes onto the Lamb modes even for relatively small NC. These figures also show that for NC of a given size, the NC modes generally contain fewer Lamb modes with larger values of l.

In Fig. 4, we project the lattice modes onto torsional Lamb modes with different values of n ($n=0,1,2$, and 3) but with the same value of $l=3$. In this case we find that, in general, the lower-order (or small values of n) Lamb modes are also eigenmodes of the discrete lattice even for small NC. However, for larger values of n the Lamb mode typically is composed of a large number of lattice modes and the Lamb model breaks down. This trend is more obvious with larger n as the size of the NC decreases.

One of the reasons for the above trends is that the wavelength of the Lamb mode becomes smaller as n increases, while the frequency of a Lamb mode can be as large as one

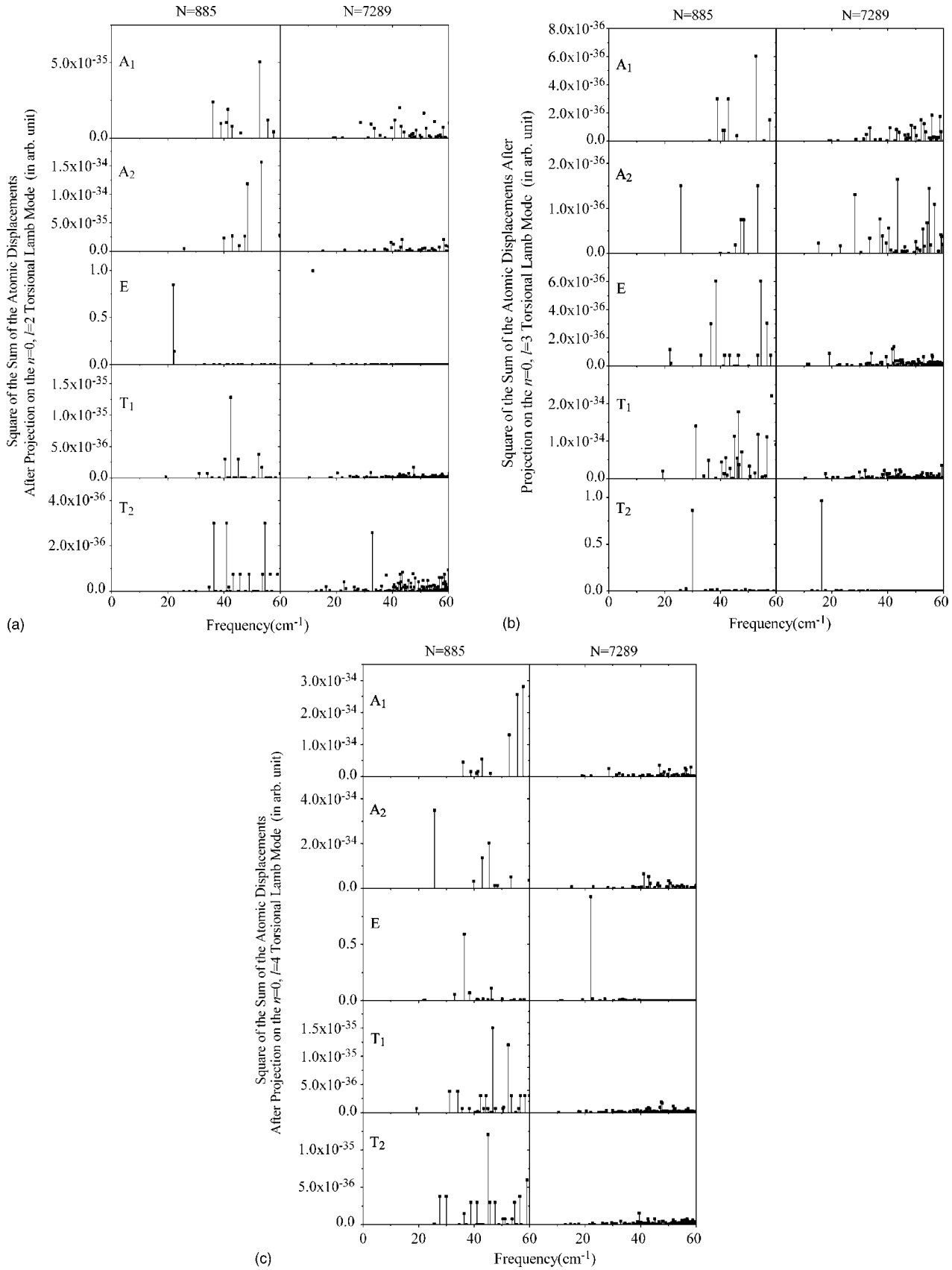

FIG. 3. The MPQ for the $n=0$ (a) $l=2$; (b) $l=3$; and (c) $l=4$ torsional Lamb modes.

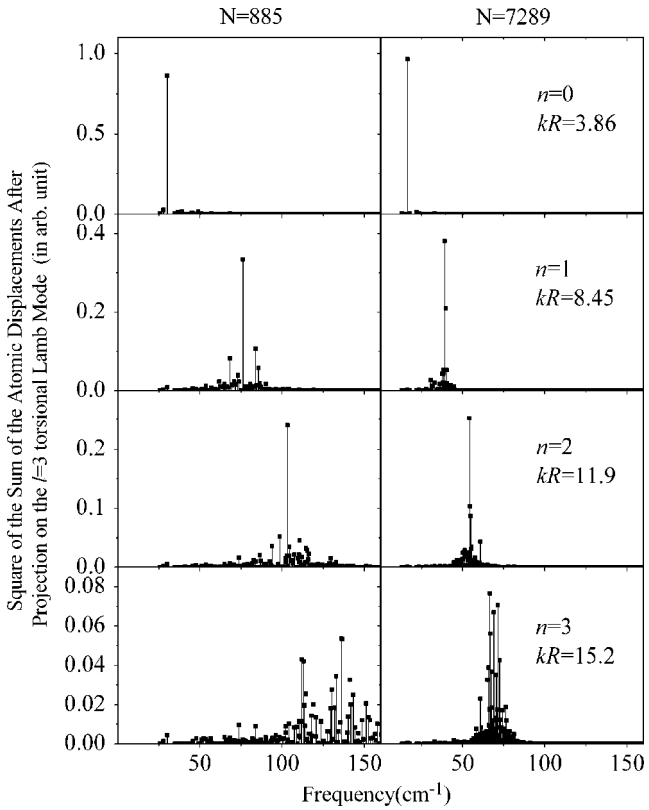

FIG. 4. The MPQ for the $l=3$ and $n=0,1,2$, and 3, torsional Lamb modes. In this figure k is related to transverse sound velocity, and R is the radius of the NC.

wants by choosing n and l large enough. However, in reality the phonon frequencies in a lattice are finite. In particular, the transverse acoustic phonons in bulk Ge have a cutoff frequency of about 100 cm^{-1} determined by the lattice constant. When the NC frequency approaches this cutoff frequency, it is impossible for a single NC lattice mode to reproduce the Lamb modes.

B. Radial amplitude distribution function of NC

To explore further the correspondence between the NC lattice modes and the Lamb modes, we further define a function which we will label as the radial amplitude distribution function (or RADF for short). The rationale behind this definition is that a spherical discrete lattice can be divided into spherical shells. Let $N_{shl}(r)$ be the number of atoms located on a shell of radius r. Next, we sum the squares of the vibration amplitudes of a specific mode over all these atoms and then divide this sum by $N_{shl}(r)$. The resultant quantity is the RADF of that particular mode for the NC mode. The RADF for the Lamb modes, on the other hand, are easily computed from the Lamb theory. For example, for the $n=0$ torsional Lamb mode RADF is $j_l^2(k_l r)$, with $k_1=5.75/R$, $k_2=2.51/R$, $k_3=3.86/R$, where R is the radius of the NC. While the RADF for the Lamb modes are continuous functions of r, the corresponding RADF tend to show fluctuations and deviations from the curve for the Lamb modes. Figure 5 shows the RADFs for the lattices modes which correspond to the

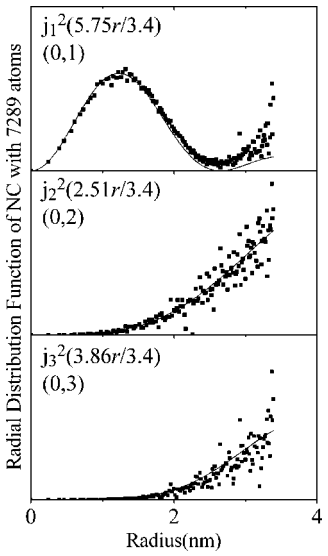

FIG. 5. The radial amplitude distribution function (RADF) of three torsional Lamb modes with (n,l) indicated in the figures. These results have been computed for a Ge NC containing 7289 atoms ($d\sim 6.8$ nm). The squares are the results for the NC, while the continuous curves represent results for the Lamb modes.

$n=0$ and $l=1,2$, and 3 torsional Lamb modes in a Ge NC with 7289 atoms (closed squares) calculated from the VFFM. For comparison, the RADF obtained from the Lamb theory are plotted as continuous curves. We can see similarity between the two sets of results in their overall dependence on r. In particular, for high values of l the mode amplitudes tend to be largest near the NC surface. In other words, the $n=0$ torsional Lamb modes with large l are essentially surface modes. However, we also notice significant difference between the lattice and Lamb modes mainly near the NC surface. The RADF of the lattice modes are often much higher than the Lamb modes near the surface. This is because atoms near the surface are less constrained in a discrete lattice model than the surface of a continuum sphere.

C. Raman intensities of NC

In Figs. 6(a)–6(c) we show the Raman intensities for the three Raman-active modes (belonging to the A_1, E, and T_2 irreducible representations, respectively) of five different-sized Ge NC calculated from the Raman polarizability with our VFFM. When compared to the corresponding phonon density of states for the same crystals published in our earlier paper,[12] it is clear that the number of Raman-active modes is a small subset of the total number of phonon modes. This result is not surprising since the number of Raman modes is expected to decrease as the crystal size becomes larger. If we assume that NC is enough for the bulk Raman selection to apply, then we expect only the zone-center modes to be Raman active. When the NC size is reduced the wave vector conservation in Raman scattering is relaxed, allowing modes of nonzero wave vector to be Raman active provided these modes have a wave vector equal to an integral multiple of (π/d), where d is the size of the NC. For the low-frequency acoustic phonon modes their dispersions are linear, so the

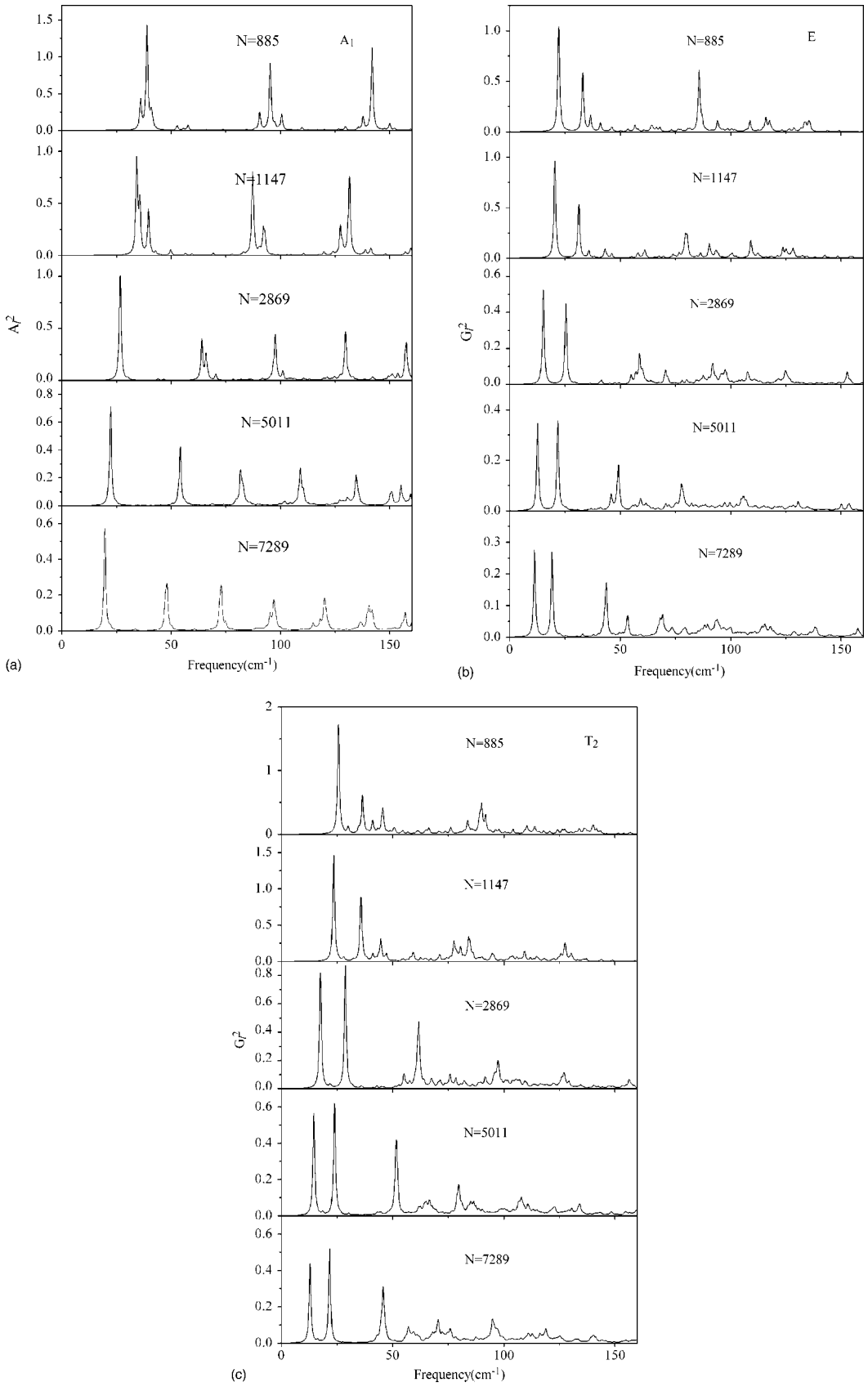

FIG. 6. The Raman intensities (the quantities A_l^2 and G_l^2 are the same as those defined in Ref. 12) of modes belonging to the (a)A_1; (b) E; and (c)T_2 irreducible representations of the T_d group.

TABLE I. Calculated Raman frequencies and intensities of a few low-frequency modes in Ge NC with N=7289 atoms. The corresponding Lamb modes obtained by projection are also listed.

Irreducible representations	Lamb mode	Frequency (cm^{-1})	Raman intensity (arbitrary unit)
A_1	$n=1$, $l=0$, spheroidal	19.6	0.904
A_1	$n=4$, $l=0$, spheroidal	47.3	0.237
A_1	$n=4$, $l=0$, spheroidal	48.1	0.316
E	$n=0$, $l=2$, torsional	11.7	0.00136
E	$n=0$, $l=2$, spheroidal	11.2	0.430
T_2	$n=0$, $l=3$, torsional	16.3	0.0197
T_2	$n=0$, $l=2$, spheroidal	12.9	0.686

frequencies of these modes will be equally spaced. As discussed in Ref. 12, this appearance of almost equally spaced modes is known as "mode folding." In Fig. 6(a), we notice that the strong Raman A_1 symmetry Raman peaks are indeed almost equally spaced. In Fig. 6(b), all the Raman spectra of E symmetry show two strong, low-frequency Raman peaks. In NC with 7289 atoms these peaks have frequencies of 11.2 and 19.1 cm^{-1}, respectively. The low-frequency Raman spectra of the T_2 symmetry modes shown in Fig. 6(c), are rather similar to the E-symmetry Raman spectra, except for their slightly higher Raman frequencies. For example, in NC with 7289 atoms the two lowest frequency Raman peaks occur at 12.9 and 21.7 cm^{-1}, respectively.

By using the projection technique described earlier, we can determine the contributions of the Raman peaks in Figs. 6(a)–6(c) to the corresponding Lamb modes. The results are summarized in Table I. From this table, we note the following important findings. (1) The strongest Raman peaks of different symmetries and polarizations in NC of a given size have comparable strengths. In the 7289 atoms NC these are the A_1 mode with frequency 19.6 cm^{-1}, the E mode with frequency 11.2 cm^{-1}, and the T_2 mode with frequency 12.9 cm^{-1}. (2) All the spheroidal modes shown in Table I are much stronger than the torsional modes, in agreement with the selection rules derived from group theory. This suggests strongly that all the experimentally observed Raman peaks in NC are due to spheroidal Lamb modes and not the torsional modes. This is in contrast to the identification of torsional Lamb modes in the crossed polarization Raman spectra suggested by many authors.[2–4] (3) The strongest Raman peak has A_1 symmetry, but this mode does not have the lowest frequency. This mode corresponds to the $n=1$ and $l=0$ spheroidal Lamb mode and is consistent with the identification of the higher-frequency Raman peak observed in the parallel polarization scattering geometry as a spheroidal Lamb mode by most authors.[2,4] (4) Experimentally the crossed polarization Raman peak was found to have a lower frequency.[2] This has been explained as a result of the lower sound speeds of transverse acoustic phonons as compared to the longitudinal acoustic phonons. We found that the lowest frequency Raman peak is of E symmetry, which should appear in the parallel polarization geometry.

The lowest frequency Raman peak appearing in the crossed polarization geometry is the 12.9 cm^{-1} T_2 mode. Projection onto the Lamb modes indicates that both of these modes contribute to the $n=0$ and $l=2$ spheroidal Lamb mode. One can consider these low-frequency E- and T_2 symmetry lattice modes as derived from the splitting of the $n=0$ and $l=2$ spheroidal modes when the NC symmetry is lowered to T_d. Similarly, the two NC modes of A_1 symmetry with almost degenerate frequencies (47.3 and 48.1 cm^{-1}) and comparable intensities also arise from splitting of the same $n=4$, $l=0$ spheroidal Lamb mode. (5) The frequencies of two E modes (11.7 and 11.2 cm^{-1}) corresponding to the $l=2$ torsional and spheroidal Lamb modes are almost degenerate. This reflects the very close values of $\eta^{(T)}=2.46$ and $\eta^{(S)}=2.64$ for $n=0$ and $l=2$ in Fig. 1. (6) For the "Raman-forbidden" torsional Lamb modes, the intensity of the $l=2$ mode is less than that of the $l=3$ mode, in agreement with the prediction of group theory. (7) The $n=0$, $l=0$ spheroidal mode has negligible Raman intensity and therefore is not shown at all in Table I.

From the above discussions, we conclude that the experimental Raman peak in the parallel polarization geometry is due to scattering from the $n=1$, $l=0$ spheroidal Lamb mode. The experimental Raman peak in the perpendicular polarization arises from the $n=0$ and $l=2$ spheroidal Lamb mode. In principle, this lower-frequency mode may by "contaminated" by an E-symmetry mode which is allowed for parallel polarization, especially since the experimental spectral resolution in these low-frequency region is often 1 cm^{-1} or larger, so that the low-frequency E- and T_2-symmetry lattice modes are not resolved. One possible explanation for the polarized nature of the experimental low-frequency mode is that we have neglected the lattice anharmonicity, which may cause the Raman-active $n=0$ and $l=2$ spheroidal Lamb mode to decay into the almost degenerate Raman-inactive torsional mode. In our previous paper we interpreted the Raman peak observed with the crossed polarization as due to the $n=0$ and $l=3$ torsional Lamb mode. We now find that the $n=0$ and $l=3$ mode may lie close to the measured peak in position, but its strength is too weak to account for the strong experimental Raman peak.

IV. SUMMARY

In summary, we have investigated in detail the low-frequency Raman spectra of spherical Ge NC with various diameters, up to about 6.8 nm, by computing the Raman polarizabilities based on a microscopic VFFM. The results are compared to the Raman selection rules for the spheroidal and torsional modes of a continuum Lamb model by using the projection method. We found that the strongest Raman peaks are due to the $l=0$ and $l=2$ spheroidal Lamb modes in agreement with the Raman selection rules. This result agrees well with the recent results of Brillouin scattering experiments in large NC.[16] When the calculated Raman intensities were compared with the Raman experimental results, we found that the Raman peaks observed in the parallel polarization scattering geometry were due to the $l=0$ spheroidal and $n=1,4,6$, etc. Lamb modes. The Raman peak with a lower frequency observed in the perpendicular polarization is also due to the $l=2$ but $n=0$ spheroidal Lamb mode. The tor-

sional Lamb modes can become Raman active when the NC size is small, but their intensities are usually much smaller than the spheroidal Lamb modes. The two Raman peaks observed experimentally and reported in Ref. 2 are the $l=0$ and $l=2$ spheroidal Lamb modes and do not involve the torsional Lamb modes as suggested by the authors.

ACKNOWLEDGMENTS

W.C. is supported by the National Natural Science Foundation of China (10275007); S.F.R. is supported by the National Science Foundation (0245648) and the Research Corporation (CC6274); and the work at Berkeley was supported in part by the Director, Office of Science, Office of Basic Energy Science, Division of Materials Sciences and Engineering, of the U.S. Department of Energy under Contract No. DE-AC03-76SF00098.

APPENDIX A: DISPLACEMENTS FOR $l=1$ SPHEROIDAL LAMB MODES

(1) $\vec{D}_{1i}^{(S)}=\nabla\phi_{1i}^{(S)}+\alpha_1\nabla\times\nabla\times\vec{A}_{1i}^{(S)}$, where $i=1,2$, and 3; $\vec{A}_{11}^{(S)}=(x,y,z)xf_1(r)$, $\phi_{11}^{(S)}=g_1(r)x$; $\vec{A}_{12}^{(S)}=(x,y,z)yf_1(r)$, $\phi_{12}^{(S)}=g_1(r)y$, and so on with

$$f_1(r)=k\frac{j_1(kr)}{(kr)} \text{ and } g_1(r)=h\frac{j_1(hr)}{(hr)},$$

$$\frac{df_1(r)}{dr}=-k^2\frac{j_2(kr)}{(kr)} \text{ and } \frac{dg_1(r)}{dr}=-h^2\frac{j_2(hr)}{(hr)},$$

$$\alpha_1=\frac{2\xi j_2(\xi)}{[-\eta j_1(\eta)+2j_2(\eta)]\eta}.$$

With these definitions, one finds

$$\nabla\times\nabla\times\vec{A}_{11}^{(S)}=\left\{2f_1(r)+r\frac{df_1(r)}{dr}\right\}\vec{i}-x\frac{df_1(r)}{dr}\left(\frac{x}{r}\vec{i}+\frac{y}{r}\vec{j}+\frac{z}{r}\vec{k}\right),$$

$$\nabla\times\nabla\times\vec{A}_{12}^{(S)}=\left\{2f_1(r)+r\frac{df_1(r)}{dr}\right\}\vec{j}-y\frac{df_1(r)}{dr}\left(\frac{x}{r}\vec{i}+\frac{y}{r}\vec{j}+\frac{z}{r}\vec{k}\right),$$

and so on.

$$\nabla\phi_{11}^{(S)}=g_1(r)\vec{i}+x\frac{dg_1(r)}{dr}\left(\frac{x}{r}\vec{i}+\frac{y}{r}\vec{j}+\frac{z}{r}\vec{k}\right),$$

$$\nabla\phi_{12}^{(S)}=g_1(r)\vec{j}+y\frac{dg_1(r)}{dr}\left(\frac{x}{r}\vec{i}+\frac{y}{r}\vec{j}+\frac{z}{r}\vec{k}\right),$$

and so on.

$\vec{D}_{11}^{(S)}$, $\vec{D}_{12}^{(S)}$, $\vec{D}_{13}^{(S)}$ belong to the T_2 or $D_u^{(1)}$ irreducible representation.

APPENDIX B: DISPLACEMENTS FOR $l=2$ SPHEROIDAL LAMB MODES

$\vec{D}_{2i}^{(S)}=\nabla\phi_{2i}^{(S)}+\alpha_2\nabla\times\nabla\times\vec{A}_{2i}^{(S)}$, where $i=1,\ldots,5$, with

$$\phi_{21}^{(S)}=g_2(r)xy,\quad \vec{A}_{21}^{(S)}=(x,y,z)xyf_2(r),\quad \phi_{22}^{(S)}=g_2(r)yz,$$

$$\vec{A}_{22}^{(S)}=(x,y,z)yzf_2(r),\ \ldots,\ \phi_{24}^{(S)}=g_2(r)[x^2-y^2],$$

$$\vec{A}_{24}^{(S)}=(x,y,z)[x^2-y^2]f_2(r),$$

and so on.

$$\nabla\phi_{21}^{(S)}=g_2(r)y\vec{i}+g_2(r)x\vec{j}+xy\frac{\vec{r}}{r}\frac{dg_2(r)}{dr},$$

$$\nabla\times\nabla\times\vec{A}_{21}^{(S)}=y\left\{3f_2(r)+\frac{(r^2-2x^2)}{r}\frac{df_2(r)}{dr}\right\}\vec{i}+x\left\{3f_2(r)+\frac{(r^2-2y^2)}{r}\frac{df_2(r)}{dr}\right\}\vec{j}-2\frac{xyz}{r}\frac{df_2(r)}{dr}\vec{k},$$

and similarly for $i=2,\ldots,5$.

$$f_2(r)=k^2\frac{j_2(kr)}{(kr)^2},$$

$$g_2(r)=h^2\frac{j_2(hr)}{(hr)^2},$$

$$\frac{df_2(r)}{dr}=-k^3\frac{j_3(kr)}{(kr)^2},$$

$$\frac{dg_2(r)}{dr}=-h^3\frac{j_2(hr)}{(hr)^2},$$

$$\alpha_2=-\frac{2[j_2(\xi)-\xi j_3(\xi)]}{[6j_2(\eta)+2\eta j_3(\eta)-\eta^2 j_2(\eta)]}.$$

$\vec{D}_{21}^{(S)}$, $\vec{D}_{22}^{(S)}$, and $\vec{D}_{23}^{(S)}$ belong to the T_2 representation, while $\vec{D}_{24}^{(S)}$ and $\vec{D}_{25}^{(S)}$ belong to the E representation. In the rotational group all five modes belong to the $D_g^{(2)}$representation.

APPENDIX C: DISPLACEMENTS FOR THE $l=2$ TORSIONAL LAMB MODES

$$\vec{A}_{21}=(x,y,z)j_2(kr)xy/r^2,$$

$$\vec{D}_{21}^{(T)}=(xz,-yz,(y^2-x^2))j_2(kr)/r^2,$$

$$\vec{A}_{22}=(x,y,z)j_2(kr)yz/r^2,$$

$$\vec{D}_{22}^{(T)}=((z^2-y^2),xy,-xz)j_2(kr)/r^2,\ldots,$$

and

$$\vec{A}_{25}=(x,y,z)j_2(kr)(2z^2-x^2-y^2)/r^2,$$

$$\vec{D}_{25}^{(T)} = (-6yz, 6xz, 0) j_2(kr)/r^2.$$

$\vec{D}_{21}^{(T)}$, $\vec{D}_{22}^{(T)}$, and $\vec{D}_{23}^{(T)}$ belong to the T_1 representation, while $\vec{D}_{24}^{(T)}$, $\vec{D}_{25}^{(T)}$ belong to E modes. In the rotational group these five modes belong to the $D_u^{(2)}$ representation.

APPENDIX D: DISPLACEMENTS FOR $l=3$ TORSIONAL LAMB MODES

$$\vec{A}_{31} = (x,y,z) j_3(kr)(x^2 - y^2)z/r^3,$$

$$\vec{D}_{31}^{(T)} = [(y^2 - x^2 - 2z^2)y, (x^2 - y^2 - 2z^2)x, 4xyz] j_3(kr)/r^3,$$

$$\vec{A}_{32} = (x,y,z) j_3(kr)(5z^2 - 3r^2)z/r^3,$$

$$\vec{D}_{32}^{(T)} = [-3(5z^2 - r^2)y, 3(5z^2 - r^2)x, 0] j_3(kr)/r^3,$$

$$\vec{A}_{33} = (x,y,z) j_3(kr)(5z^2 - r^2)x/r^3,$$

$$\vec{D}_{33}^{(T)} = [-10xyz, (10x^2 - 5z^2 + r^2)z, (5z^2 - r^2)y] j_3(kr)/r^3,$$

$$\vec{A}_{34} = (x,y,z) j_3(kr)(5z^2 - r^2)y/r^3,$$

$$\vec{D}_{34}^{(T)} = [(5z^2 - 10y^2 - r^2)z, 10xyz, -(5z^2 - r^2)x] j_3(kr)/r^3,$$

$$\vec{A}_{35} = (x,y,z) j_3(kr)(3xy^2 - x^3)/r^3,$$

$$\vec{D}_{35}^{(T)} = [6xyz, 3(x^2 - y^2)z, 3(y^2 - 3x^2)y] j_3(kr)/r^3,$$

$$\vec{A}_{36} = (x,y,z) j_3(kr)(3x^2y - y^3)/r^3,$$

$$\vec{D}_{36}^{(T)} = [3(x^2 - y^2)z, -6xyz, 3(3y^2 - x^2)x] j_3(kr)/r^3,$$

$$\vec{A}_{37} = (x,y,z) j_3(kr)xyz/r^3,$$

$$\vec{D}_{37}^{(T)} = [x(z^2 - y^2), y(x^2 - z^2), z(y^2 - x^2)] j_3(kr)/r^3.$$

$\vec{D}_{31}^{(T)}$, $\vec{D}_{32}^{(T)}$, $\vec{D}_{33}^{(T)}$, $\vec{D}_{34}^{(T)}$, $\vec{D}_{35}^{(T)}$, $\vec{D}_{36}^{(T)}$ belong to the $T_1 + T_2$ representations, while $\vec{D}_{37}^{(T)}$ belongs to the A_2 representation. In the rotation group all seven modes belong to the $D_g^{(3)}$ representation.

[1] A. D. Yoffe, Adv. Phys. **42**, 173 (1993); A. D. Yoffe, *ibid.* **50**, 1 (2001).
[2] N. N. Ovsyuk, E. B. Gorokhov, V. V. Grishchenko, and A. P. Shebanin, JETP Lett. **47**, 298 (1988).
[3] A. Tanaka, S. Onari, and T. Arai, Phys. Rev. B **47**, 1237 (1993).
[4] B. Champagnon, B. Andrianasolo, and E. Duval, Mater. Sci. Eng. B **9**, 417 (1991).
[5] H. Lamb, Proc. London Math. Soc. **13**, 189 (1882).
[6] W. A. Harrison, *Electronic Structures and the Properties of Solids* (Freeman, San Francisco, 1980).
[7] W. Cheng, S. F. Ren, and P. Y. Yu, Phys. Rev. B **68**, 193309 (2003).
[8] S. F. Ren, Z. Q. Gu, and D. Y. Lu, Solid State Commun. **113**, 273 (2000).
[9] S. F. Ren, D. Lu, and G. Qin, Phys. Rev. B **63**, 195315 (2001).
[10] G. Qin and S. F. Ren, J. Appl. Phys. **89**, 6037 (2001).
[11] G. Qin and S. F. Ren, Solid State Commun. **113**, 273 (2000).
[12] W. Cheng and S. F. Ren, Phys. Rev. B **65**, 205305 (2002).
[13] S. F. Ren and W. Cheng, Phys. Rev. B **66**, 205328 (2002).
[14] E. Duval, Phys. Rev. B **46**, 5795 (1992).
[15] Michael Tinkham, *Group Theory and Quantum Mechanics* (McGraw-Hill, New York, 1964).
[16] M. H. Kuok, H. S. Lim, S. C. Ng, N. N. Liu, and Z. K. Wang, Phys. Rev. Lett. **90**, 255502 (2003).